

Erosion and Flooding—Threats to Coastal Infrastructure in the Arctic: A Case Study from Herschel Island, Yukon Territory, Canada

Boris Radosavljevic^{1,2}  · Hugues Lantuit^{1,2} · Wayne Pollard³ · Paul Overduin¹ · Nicole Couture⁴ · Torsten Sachs⁵ · Veit Helm⁶ · Michael Fritz¹

Received: 20 February 2015 / Revised: 9 October 2015 / Accepted: 27 October 2015
© The Author(s) 2015. This article is published with open access at Springerlink.com

Abstract Arctic coastal infrastructure and cultural and archeological sites are increasingly vulnerable to erosion and flooding due to amplified warming of the Arctic, sea level rise, lengthening of open water periods, and a predicted increase in frequency of major storms. Mitigating these hazards necessitates decision-making tools at an appropriate scale. The objectives of this paper are to provide such a tool by assessing potential erosion and flood hazards at Herschel Island, a UNESCO World Heritage candidate site. This study focused on Simpson Point and the adjacent coastal sections because of their archeological, historical, and cultural significance. Shoreline movement was analyzed using the Digital Shoreline Analysis System (DSAS) after digitizing shorelines from 1952, 1970, 2000, and 2011. For purposes of this analysis, the coast was divided in seven coastal reaches (CRs) reflecting different morphologies and/or exposures. Using linear regression rates obtained from these data, projections of

shoreline position were made for 20 and 50 years into the future. Flood hazard was assessed using a least cost path analysis based on a high-resolution light detection and ranging (LiDAR) dataset and current Intergovernmental Panel on Climate Change sea level estimates. Widespread erosion characterizes the study area. The rate of shoreline movement in different periods of the study ranges from -5.5 to 2.7 $\text{m}\cdot\text{a}^{-1}$ (mean -0.6 $\text{m}\cdot\text{a}^{-1}$). Mean coastal retreat decreased from -0.6 $\text{m}\cdot\text{a}^{-1}$ to -0.5 $\text{m}\cdot\text{a}^{-1}$, for 1952–1970 and 1970–2000, respectively, and increased to -1.3 $\text{m}\cdot\text{a}^{-1}$ in the period 2000–2011. Ice-rich coastal sections most exposed to wave attack exhibited the highest rates of coastal retreat. The geohazard map combines shoreline projections and flood hazard analyses to show that most of the spit area has extreme or very high flood hazard potential, and some buildings are vulnerable to coastal erosion. This study demonstrates that transgressive forcing may provide ample sediment for the expansion of depositional landforms, while growing more susceptible to overwash and flooding.

Communicated by David Reide Corbett

✉ Boris Radosavljevic
boris.radosavljevic@awi.de

¹ Research Unit Potsdam, Alfred Wegener Institute, Helmholtz Centre for Polar and Marine Research, Potsdam, Germany

² Institute of Earth and Environmental Science, University of Potsdam, Potsdam, Germany

³ Department of Geography and Centre for Climate and Global Change Research, McGill University, Montreal, Canada

⁴ Northern Canada Division, Geological Survey of Canada, Ottawa, Canada

⁵ GFZ German Research Centre for Geosciences, Potsdam, Germany

⁶ Alfred Wegener Institute for Polar and Marine Research, Helmholtz Centre for Polar and Marine Research, Bremerhaven, Germany

Keywords Arctic · Coastal erosion · UNESCO · Vulnerability mapping · Permafrost coasts

Introduction

Continuing sea level rise (SLR) and the declining extent and duration of sea ice and landfast ice render Arctic coasts increasingly vulnerable to coastal erosion, a region where warming exceeds the global mean (Hartmann et al. 2013; Serreze and Barry 2011). The occurrence of severe storms is expected to increase, as well (Lambert 2004). Although circumpolar trends have not been observed (Overduin et al. 2014), multiple studies in the Alaskan Beaufort Sea indicate that erosion has intensified in recent decades (e.g., Barnhart et al. 2014a; Jones et al. 2009; Mars and Houseknecht 2007).

All these facts present mitigation challenges since these natural processes (e.g., erosion) infringe on a site of human activity and present a serious hazard. Shoreline recession hazards to coastal settlements (Forbes 2011; Mackay 1986; Maslakov and Kraev 2014; Mason et al. 2012) and archeological sites (Friesen and Arnold 2008; Westley et al. 2011) have been documented across the Arctic. In this study, we present an assessment of sea level rise, shoreline recession, and flooding on Simpson Point (Fig. 1), a gravelly spit on Herschel Island, Yukon Territory, Canada. Using shoreline retreat rates, topographic information and scenarios of coastal flooding, we present a map of coastal geohazards.

An inherent characteristic of the global climate system is the disproportionately high temperature variability in the Arctic compared to lower latitudes; a

phenomenon known as Arctic amplification. This phenomenon is documented in instrumental and paleoclimatic records and in climate model projections (Serreze and Barry 2011). As a result of the increase in mean sea surface temperature in the Arctic Ocean, the melt season lengthened by 5 days per decade from 1979 to 2013 (Stroeve et al. 2014). Over the same time period, the decline in sea ice extent and thickness accelerated (Kwok and Rothrock 2009; Stroeve et al. 2007, 2014, 2012). The increasing open water area and duration dramatically influence wave climates, which together with greater storm frequency and magnitude allow for larger waves to develop and generally result in higher energy coastal systems (Church et al. 2013; Thomson and Rogers 2014). When coupled with the

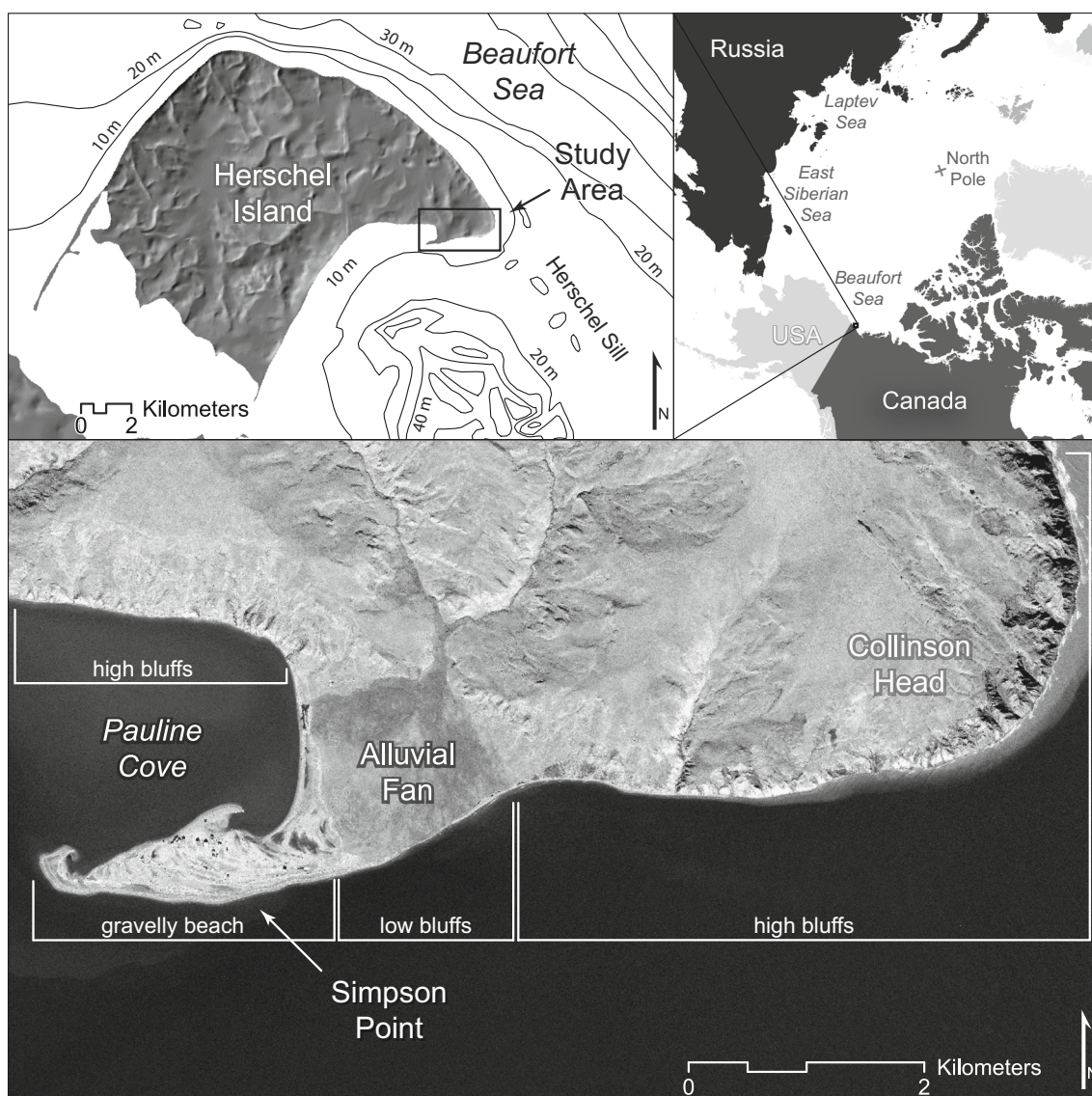


Fig. 1 Herschel Island is located in the southern Beaufort Sea in Canada. The regional overview shows Herschel Island and bathymetry. The extent of the study area is shown in the map on the *bottom*, together with coastline characteristics

unique character of permafrost coasts, these conditions tend to hasten shoreline retreat (Jones et al. 2009; Manson and Solomon 2007; Overeem et al. 2011).

Coastal evolution in the Arctic is driven by a combination of relative SLR, factors related to climatic variability, and morphosedimentary features of the coast (Manson and Solomon 2007). During the 20th century, mean global sea level rose at a rate of $1.7 \text{ mm}\cdot\text{a}^{-1}$, accelerating to $3.2 \text{ mm}\cdot\text{a}^{-1}$ in the past two decades (Meyssignac and Cazenave 2012). The maximum probable rate of SLR in the Canadian Beaufort Sea is reported at $2.5 \text{ mm}\cdot\text{a}^{-1}$ (Hill et al. 1985). At the Tuktoyuktuk tide gauge, the rate is $3.5 \text{ mm}\cdot\text{a}^{-1}$ (Manson and Solomon 2007); however, this figure incorporates $-1.68 \text{ mm}\cdot\text{a}^{-1}$ of submergence due to glacial isostatic adjustment and correction for ice-mass changes (James et al. 2014). At Herschel Island, SLR may be as high as ca. $3 \text{ mm}\cdot\text{a}^{-1}$ (S. Blasco, personal communication). Projections of mean sea level elevations at the end of the twenty-first century vary from 0.26 to 0.98 m (Church et al. 2013). However, due to atmospheric changes and increases in freshwater input, the rate of relative SLR in the Arctic is likely to be higher than the global average (Church et al. 2013). One consequence of SLR is increased occurrence of coastal flooding (Walsh et al. 2010).

Even though the Arctic coasts are frozen for 9 months of the year, erosion rates are comparable to lower latitudes, and a significant proportion of the coasts in the Arctic Coastal Dynamics Database is erosional (Lantuit et al. 2012). Growing fetch (length, width, and area), especially when it is concurrent with storm activity in September and October, is predicted to generate greater storm surge and wave setup (Dumas et al. 2005; Thomson and Rogers 2014). Return frequency of flood levels, however, are usually not available as such data are rarely collected. An analysis of driftwood strand line elevations at Tuktoyuktuk (ca. 280 km east of Herschel Island) reports surge elevations of up to 2.4 m above mean water level (Harper et al. 1988), an area where numerical modeling predicts an amplification of surge levels (Henry 1975).

The first step in risk mitigation is achieved by defining vulnerable areas and appropriately managing these areas (Danard et al. 2003). This study aims to determine how ongoing and projected climatic and sea level changes will affect the historic settlement area on Simpson Point, in particular by quantifying the hazard potentials related to coastal erosion and flooding and identifying sites that would potentially be endangered by these processes. A previous study on Herschel Island quantified coastal erosion rates (Lantuit and Pollard 2008) but did not consider the shoreline dynamics of Simpson Point. Maps of SLR sensitivity on a continental scale exist for the Canadian Arctic (Shaw et al. 1998), and a project to assess coastal geohazards at a scale of 1:50,000 is under development (Couture et al. 2013), yet the scale of these products limits their value locally. Examples of high-resolution

coastal geohazard maps in Canada and the USA are available from Northern Newfoundland (Westley et al. 2011) or from the barrier islands of the Texas coast (TAMUCC-HRI 2014). These maps are valuable tools for coastal decision makers, and this study provides such an assessment for the historic settlement area on Simpson Point.

Study Area

The study area encompasses the NE coastal portion of Herschel Island ($69^{\circ} 36' \text{ N}$; $139^{\circ} 04' \text{ W}$) (Fig. 1), a stretch of coast characterized by eroding cliffs, gullies, retrogressive thaw slump features, an alluvial fan, and a drift-aligned coarse clastic spit. The geometry of these features has resulted in a natural harbor named Pauline Cove. The main focus of this study is Simpson Point, a gravelly spit that forms the eastern border to Pauline Cove (Figs. 1 and 2). Herschel Island is part of an ice push moraine, formed during the farthest advance of the Laurentide Ice Sheet to the west during the Wisconsin Glaciation (Fritz et al. 2012; Mackay 1959; Rampton 1982). It is located in the southern Beaufort Sea, about 2 km off the mainland coast of the Yukon Territory, Canada. The island consists of perennially frozen marine and glacial sediments, characterized by rolling topography with a maximum elevation of 183 m asl (Lantuit and Pollard 2008).

Herschel Island is not permanently inhabited today but remains an important cultural and archeological site as reflected by its inclusion in the Inuvialuit Final Agreement which was signed in 1984. Simpson Point is the location of a historic whaling settlement, as well as many archeological sites. Whalers arrived in the late 1800s; however, human occupation of the island began much earlier, with the first Inuvialuit arriving about 800 years ago, while hunters visited the



Fig. 2 Oblique photograph of the historic whaling settlement on Simpson Point, Herschel Island (photo: W. Pollard, 2007)

surrounding areas, and probably Herschel Island, during the past 10,000 years (Nagy 2012, p. 146). The island is an important cultural site for the Inuvialuit and draws many tourists and scientists to this location. Since 1987, Herschel Island has been a Yukon Territorial Park jointly managed by the Yukon Government and the Inuvialuit. In recognition of its archeological, cultural, esthetic, and biological value, Herschel Island is a candidate for a UNESCO World Heritage site (UNESCO 2013). Coastal changes in the Arctic often threaten coastal infrastructure (Mackay 1986; Mason et al. 2012). On Herschel Island, coastal erosion has forced the relocation of buildings (Olynyk 2008, p. 212), while a Thule Eskimo dwelling site was lost to coastal erosion (Morgan et al. 1983).

For the purposes of this study, the shoreline was subdivided into different coastal reaches (CRs), reflecting common morphology and/or orientation (Table 1). The dominant coastal morphology in this study is ice-rich bluffs (25–35 m in height) fronted by a narrow beach (Harper 1990) (CRs 1, 2, and 7). The bluffs are composed of fine-grained diamicton and characterized by widespread ground ice that reaches up to 60–70 % by volume in the upper 10–15 m (Pollard 1990). These ice bodies exhibit thicknesses ranging from 4 to 20 m (Fritz et al. 2011; Pollard 1990). These coastal sections exhibit landscape features indicative of high ground ice contents, i.e., retrogressive thaw slumps (Pollard 2005). The bluffs are subject to gullying resulting from thawing of exposed permafrost (thermo-denudation), while CR1 is also undergoing creep or solifluction-related subsidence expressed in faulting with an approximate NW-SE strike. Consequently, the drainage areas for gullies discharging at the foot of the cliff is larger, and the gullies, wider. CRs 1, 2, and 7 are also subject to cliff collapse (Fig. 3b), caused by thermoabrasional notching of the cliff base through the combined action of thermal and mechanical energy of the sea (Aré 1988; Günther et al. 2013). The alluvial fan (CR3) is composed of an upward fining sequence of gravel, sand, and silt, up to 8 m in thickness (Bouchard 1974). The mean elevation of CR3 is 3.1 m, with ice contributing up to 40 % to the volume (Obu et al. accepted). Wetland vegetation on the alluvial fan reflects high soil moisture (Smith et al. 1989); standing and flowing water have been observed. Block failure has also been observed along the alluvial fan shoreline (Fig. 3a). At Simpson Point, a large spit progrades

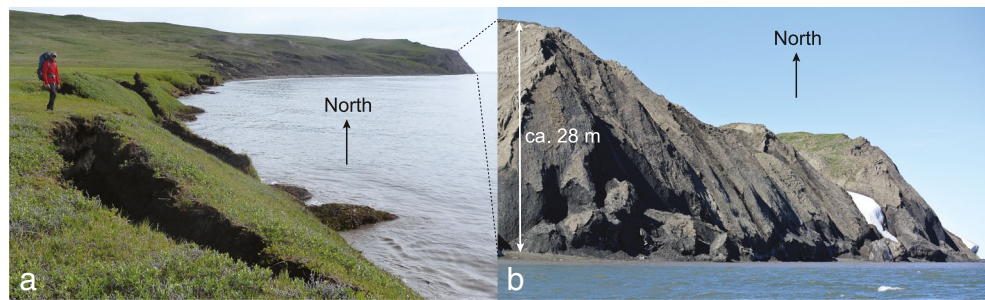
from the southern edge of the alluvial fan. It is composed of coarse clastic sediments, is about 870 m long, and covers an area of ~15 ha (CR4–5). Our data indicate that spit elevations do not exceed 1.2 m above sea level (asl), while mean elevations of CRs 4 and 5 are 0.4 and 0.3 m, respectively. No ground ice is reported in the upper meter of soil (Obu et al. accepted). The spit topography is marked by low ice-push ridges and storm berms, with remnant shorelines delineating the progradation of the spit. Westerly longshore drift initially formed an offshore bar which evolved into a cusped foreland and gradually grew into the modern spit (Smith et al. 1989). The spit is a dynamic feature, its stability fundamentally a function of sea level change, wave climate, and sediment supply (Carter and Orford 1993; Forbes et al. 1995). Periods of stability may be punctuated by extreme events that significantly alter the morphology of the spit and transport sediment in the cross-shore direction. Although vertical accretion of the barrier caused by overwash may make it less susceptible to flooding and SLR, such events may be disastrous for anthropogenic features on the spit. CR6 entails the low-lying beach at the head of Pauline Cove, with a mean elevation of 0.7 m. Ground ice does not comprise a significant component of the beach sediments, as was the case in the adjacent spit.

The Arctic climate at Herschel Island is characterized by long, cold winters and relatively short summers. Weather data were collected at Herschel Island from 1899 to 1905, while an automatic weather station was installed in 1995 (Burn and Zhang 2009). The mean annual air temperature and precipitation are approximately -12 °C and 155 mm, respectively, based on Environment Canada records for Komakuk Beach (ca. 50 km west of Simpson Point). The coldest month is February with a mean monthly temperature of -24.7 °C (Burn and Zhang 2009). Winds profoundly affect nearshore dynamics, influencing waves, astronomical tides, nearshore currents, and ice processes. The presence of seasonal ice limits the wave energy in this area. Open water conditions typically occur from June to early October when fetches often exceed 100 km (Héquette and Barnes 1990; Solomon 2005). During the 2009 to 2012 open water seasons, prevailing winds were typically from the SSE, reaching maximum average hourly speeds of 46 km h⁻¹ at Herschel Island (mean 18.7, standard deviation 8.3) (Environment Canada, <http://climate.weather.gc.ca/>). Dominant NW winds reached maximum hourly

Table 1 Coastline reach characteristics

Reach	1	2	3	4	5	6	7
Landform	High bluffs	High bluffs	Low tundra bluffs, alluvial fan	Barrier spit	Barrier spit	Beach	High bluffs
Material	Diamicton	Diamicton	Silt, sand, gravel	Sand, gravel	Sand, gravel	Sand, gravel	Diamicton
Shoreline length (m)	1848	1240	846	711	340	637	895
Orientation	ENE	S	SSE	S	NNW	W	SSW

Fig. 3 Block failure on the alluvial fan shoreline in CR3 (a), and steep bluffs exhibiting block failures characteristic of CRs 1, 2, and 3 (b)



speeds of 67 km h^{-1} (mean 19.8, standard deviation 10.9) (Fig. 4). Storms become more frequent in late August and September and are from the NW and to a lesser extent from the SSE (Solomon 2005). In the Beaufort Sea, fetch length may exceed 1000 km in September (Thomson and Rogers 2014), and significant wave heights may exceed 4 m, with wave periods up to 10 s (Pinchin et al. 1985). Herschel Sill, a submerged linear feature with a SE strike extends from Collinson Head to Kay Point on the mainland, serves as a node for landfast ice formation (i.e., Thetis Bay is covered by landfast ice during winter)..

The Beaufort Sea is microtidal (0.3–0.5 m); however, winds are an important factor in modulating the astronomical tide (Héquette et al. 1995; Héquette and Barnes 1990). Northwesterly winds create a positive surge, in contrast to easterly winds which cause a negative surge.

Methods

Shoreline Mapping and Analysis

Given the remoteness of the study area, there is limited availability of high-quality vertical aerial photographs needed to extract past shorelines. Consequently, shoreline dynamics were assessed by digitizing shoreline positions using sets of $22.9 \times 22.9 \text{ cm}$ ($9 \times 9 \text{ inch}$) aerial photographs taken in 1952 and 1970, and satellite images from 2000 and 2011. Digital copies of the historic imagery were scanned by the Canadian National Air Photo Library (NAPL) at 1500 dpi. Information about scale and resolution of imagery used for this study is listed in Table 2.

The images were processed using a softcopy photogrammetric method with PCI Orthoengine and co-registered to the 2011 image and a 2-m digital elevation model (DEM) based on Ikonos stereo couples from 2004 to reduce distortion from lens, camera attitude, Earth curvature, and terrain relief. The 2011 image was registered using differential global positioning system (DGPS)-surveyed ground control points as reported in Lantuit and Pollard (2008). All images were orthorectified assuming a flat terrain, which would lead to minimal distortion of the image at sea level. Depending on

the image quality and definition, shorelines were mapped to the wet-dry line at a scale of 1:600.

Shoreline position statistics were calculated with the USGS Digital Shoreline Analysis System (DSAS) extension for ESRI ArcGIS (Thieler et al. 2009), using shore normal transects at 5 m spacing. The more dynamic areas corresponding to the prograding spit ends were excluded from this analysis, we did, however, assess the changes in length by casting a transect across the western tip of the spit. DSAS is capable of producing various shoreline movement statistics while accounting for uncertainty in the analysis to provide statistical robustness (Thieler et al. 2009). Sources of shoreline uncertainty may include pixel, digitization, rectification, seasonal, and tidal fluctuation errors (Romine et al. 2009). This study addressed pixel, digitizing, and rectification errors (see Table 2).

The pixel error refers to the spatial resolution of an image. This corresponds to the image resolution in digital

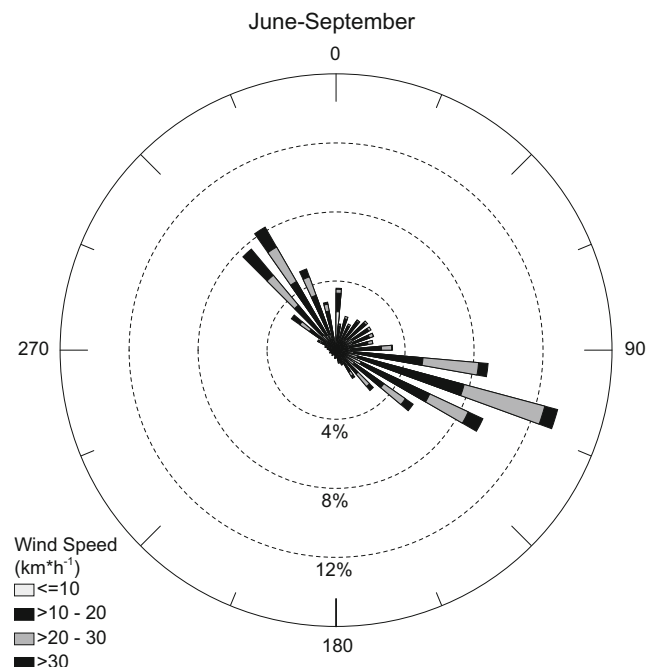


Fig. 4 Wind direction and speed frequency in the ice-free period (June–September), observed at the weather station on Simpson Point, Herschel Island, from 2009 to 2012

Table 2 Shoreline uncertainties are a combination of root mean square error (RMS) related to differences in location of ground control points (GCPs), image quality, and shoreline mapping

Date	Images	Image type	Scale	GCPs	Georeferencing RMS (m)	Pixel error (m)	Digitizing Error (m)	Total shoreline error (m)
August 28, 1952	1	B/W aerial	1:70 000	8	2.9	3.5	0.7 (0.3)	7.0 (0.3)
August 20, 1970	3	B/W aerial	1:12 000	19	1.7	0.6	0.5 (0.6)	2.7 (0.7)
September 18, 2000	1	Ikonos		15	0.9	1.0	0.8 (0.6)	2.6 (0.6)
August 31, 2011	1	GeoEye			Base image	0.5	0.4 (0.3)	0.9 (0.3)

Mean uncertainties are given with standard deviations in parentheses

photographs. The resolution, or sharpness, of aerial photographs is a combined function of the film and the camera lens. The resolution is usually determined by photographing a target containing a test pattern of line pairs (lp) of equal width and separation. This information was not provided by the NAPL. However, a typical aerial photogrammetric camera with a 9×9 -in. format is capable of resolving 20–40 lp per millimeter, and the ground resolution (GR) can be determined using Eq. 1 (Lo et al. 2007, pp. 291–292).

$$GR = w \times SF \quad (1)$$

where w is the width in millimeters of one line pair and SF is the scale factor of the photograph. The worst case estimate was used to assess the pixel error of the aerial photographs in this study and ranged between 0.5 and 3.5 m.

Uncertainty of a shoreline position stemming from interpretation is termed digitizing error. In particular, it refers to the standard deviation of shoreline position interpreted by different analysts. In this study, a single operator digitized each shoreline three times. Intersects of these shorelines were derived from perpendicular transects at 1 m spacing. A midpoint was calculated at each transect from which a mean shoreline was constructed for further analysis. The mean distance of the constructed midline to the transect intersects was calculated for every 50-m section of shoreline. The corresponding digitizing error ranged from 0 to 3.8 m, with the greatest offsets corresponding to shorelines obscured by cliff shadows.

PCI Orthoengine reports the quality of the math models used in the rectification process as a root mean square (RMS) of the residual. Rectification error in this project was generally <3.0 m.

DSAS provides a number of different shoreline statistics (e.g., end point rate (EPR), linear regression rate (LRR), weighed linear regression (WLR)). Shoreline retreat rates in this study are given in EPR for comparison between time steps and as LRR for the whole time period of the study. Negative rates correspond to landward movement of the shoreline, i.e., erosion. EPR is calculated by taking the distance from the oldest to the

most recent shoreline divided by the elapsed time (Thieler et al. 2009), as shown in Eq. 2.

$$EPR = \frac{\text{distance in meters}}{\text{time between oldest and most recent shoreline}} \quad (2)$$

The advantage of the EPR method is that it is relatively simple. Its limitations are that only two end points are used; thus, reversals, or magnitude changes, and cyclical trends in shoreline movement may be missed (Genz et al. 2007; Thieler et al. 2009). We compared the different statistics with the EPR for the period 1952–2011 and found that EPRs were consistently more conservative than other statistics, such as LRR and WLR. This may be indicative of a magnitude change because EPR only takes into account the oldest and the most recent shoreline. Nevertheless, we chose the method as it has been applied in previous studies in the Canadian Beaufort Sea (e.g., Lantuit and Pollard 2008; Solomon 2005). Foster and Savage (1989) computed the minimum time between shoreline position to include in their method of calculating the average long-term rate of change.

$$T = \frac{\sqrt{(E_1)^2 + (E_2)^2}}{R} \quad (3)$$

where T is the time between the first and second datasets, and E_1 and E_2 correspond to uncertainties associated with the respective dataset, and R denotes the rate of shoreline movement. In the course of the analyses, we calculated EPRs for the periods 1952–1970, 1970–2000, and 2000–2011. We compared the EPRs statistically, eliminating rates of change that were smaller than the associated uncertainty by solving the above equation for R .

Long-term shoreline change was assessed using a linear regression approach. This method uses all available data irrespective of trend or accuracy. The method is susceptible to outlier effects and is sensitive to uneven point distribution or

point clusters. Although this method may underestimate the rate of shoreline movement (Dolan et al. 1991) because the time step between the last two data points is small, these points should have a greater influence on the LRR and, thus, reflect recent conditions more closely. All data points were used in statistical summaries of the LRR.

Changes in coastal reach area for the time periods analyzed were assessed by creating polygons delimited by shorelines of respective time steps in ArcGIS.

Vulnerability Assessment

We present a vulnerability assessment for the historic area of Simpson Point where hazards are defined as something that may potentially be dangerous or harmful (Huder 2012). In the context of coastal hazards, hazards are naturally occurring processes that threaten infrastructure and human life. Vulnerability refers to the exposure to a specific hazard (Füssel 2007). For our purposes, we limited the assessment to hazards stemming from shoreline change and coastal flooding.

In order to assess the vulnerability of Simpson Point to shoreline retreat, we used the linear regression rates (LRR) for the period of 1952–2011 and projected those rates along the same transects they originated from and where they crossed the 2011 shoreline, 20 and 50 years into the future, respectively. The projection time frames match the time frames used in the flooding hazard assessment discussed later in this section. The LRR was chosen over other shoreline movement calculations because all shoreline positions are considered in the calculation, and more weight is given to more recent shorelines due to a smaller time increment.

Coastal flooding vulnerability was assessed using the cost distance analysis tool in ArcGIS. A cost distance analysis calculates the distance of each cell on a cost surface to the input source. Input sources were defined using the shoreline and elevation data. Cost is analogous to the difficulty of water reaching a certain point on the spit in case of flooding. A cost surface was created from an airborne light detection and ranging (LiDAR) digital elevation model and a derived slope raster. LiDAR data were obtained in 2013 during an overflight of the Alfred Wegener Institute Polar 5 research aircraft using a RIEGL VQ-580. These data have a point spacing of <1 m. Low-pass filtering was used to remove spikes in LiDAR data. This dataset was gridded to a 1-m resolution. We used a standard normal deviate approach to normalize differences in magnitude between the elevation and slope datasets. Equal weighing was given to both elevation and slope. The cost distance analysis allows different weights to be attached to input sources. The sea was defined by the 2011 shoreline and weighed at 1, while areas defined by the 0 m contour located on the spit defined sources weighed at 0.5. The

internal sources were deemed necessary because the spit is composed of gravelly sands with high hydraulic conductivity.

The resulting cost distance raster was classified based on projections of sea level rise in 20 and 50 years, based on representative concentration pathways (RCPs) 2.6 and 8.5 (Church et al. 2013). These represent low- and high-end estimates of global sea level rise made by the Intergovernmental Panel on Climate Change (IPCC). In 2031, the RCP projections of sea level are very similar (0.39 ± 0.03 and 0.4 ± 0.04 m, respectively), while in 2061, sea level for RCP2.6 and RCP8.5 is at 0.53 ± 0.08 and 0.6 ± 0.11 m, respectively. There is no tide gauge and thus no established sea level at Herschel Island. Sea level elevation was derived from the LiDAR data, as no anomalous water level was observed in the field. Based on the RCPs, we created polygons with elevation ranges that defined different hazard typologies and classified the cost distance raster in Exelis ENVI:

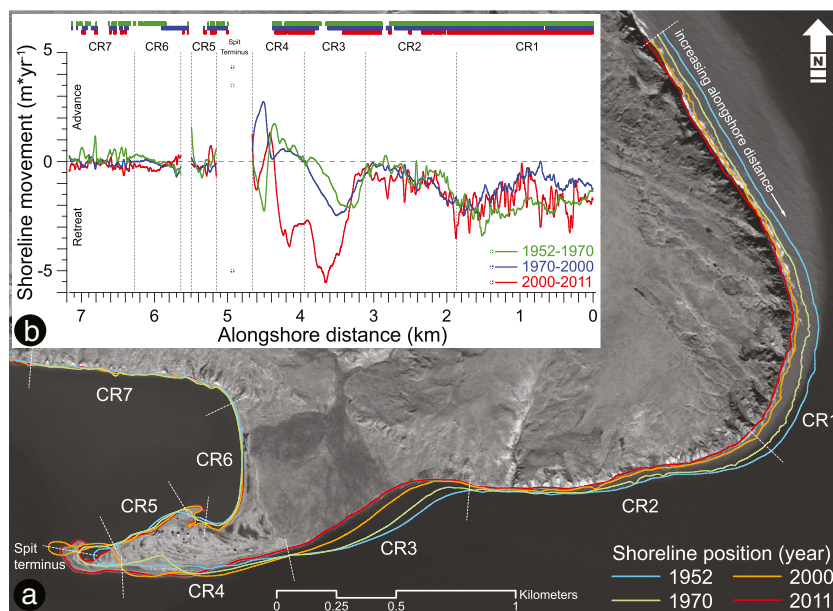
1. Extreme: elevation range 0–0.36 m. Areas subject to very frequent flooding, for water levels up to the lower RCP estimate
2. High: elevation range 0.36–0.45 m. Areas subject to frequent flooding, incorporating the range of sea level projections by RCP2.6 and RCP 8.5 in 2031
3. Moderate: elevation range 0.45–0.71 m. Areas subject to flooding with water levels matching the range of RCP2.6 and RCP8.5 sea level projections in 2061
4. Low: elevations above 0.71 m. Areas subject to flooding with water levels exceeding the 50-year sea level projection

Results

Shoreline Movement

Shorelines were digitized and EPRs were calculated using shorelines from 1952, 1970, 2000, and 2011 (Fig. 5). Uncertainties were accounted for, as summarized in Table 2. Negative values in this study indicate landward movement of the shoreline, i.e., erosion and positive values seaward shoreline advance. After eliminating shoreline movement rates smaller than the minimum (Eq. 3), we compared EPRs for different time periods statistically (Table 3 and Fig. 6). The data show erosion in almost all CRs across all time periods. A significant deceleration of erosion between 1952 and 1970 and 1970–2000 using a paired *t* test ($t = -9.54$, $df = 776$, p value = 0). Erosion significantly increased between 1970 and 2000 and 2000–2011 ($t = 22.37$, $df = 934$, p value = 0). We noted significant landscape changes including reactivation of

Fig. 5 **a** Study area showing historic shoreline positions and different coastal reaches (CR1–7). CRs differ in morphology and location and are numbered 1–7. **b** Rates for different time periods. Colored bars at the top of the graph indicate the rate exceeded the minimum requirement for statistical treatment



retrogressive thaw slumps and gullies and drainage of polygonal wetlands in the 1970s imagery. In total, a net loss of ca. -31.1 ha of coastal area loss occurred over the time period of the study, a mean loss of -0.53 ha \cdot a $^{-1}$.

CR1 lies to the north of Collinson Head, where exposure to coastal processes is highest. Overall, this section is characterized by erosion and underwent the most rapid mean retreat in the period 1952–1970 or -2.1 ± 0.4 m \cdot a $^{-1}$. Overall, erosion was fairly uniform spatially (Fig. 6), with the highest erosion rates (-3.0 m \cdot a $^{-1}$ or more) occurring close to the bend where a large gully drains some polygonal wetlands and thermokarst inland and decreasing further SW. In the period 1970–2000, a deceleration of retreat took place, with a mean retreat rate of -1.2 ± 0.5 m \cdot a $^{-1}$, accelerating in

2000–2011 to -1.8 ± 0.6 m \cdot a $^{-1}$. Over the period of the study (1952–2011), the shoreline retreated 91.9 ± 21.7 m, on average, with the greatest erosion rates and area loss (ca. 18 ha) affecting the bend of the headland (Fig. 6).

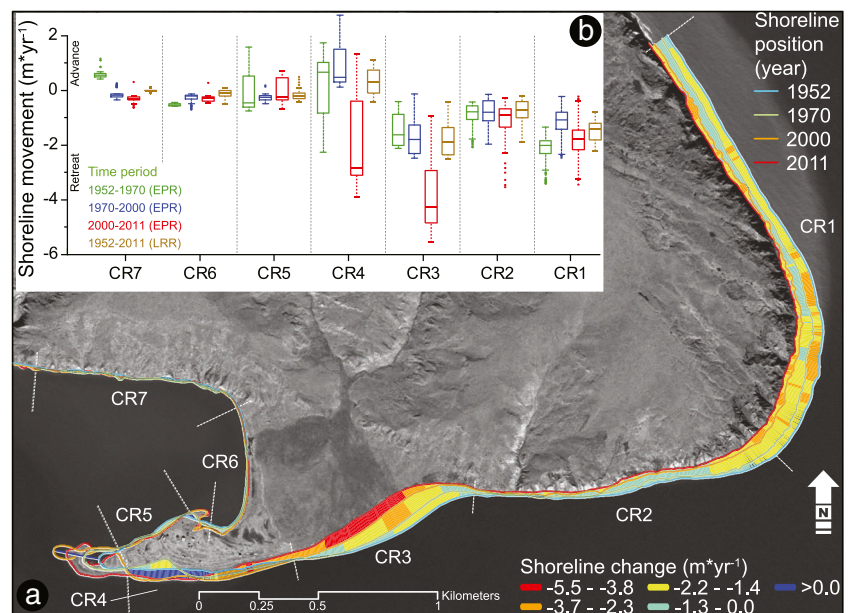
CR2 is somewhat less exposed to wave attack generated by predominant NW winds, given its orientation to the south and the presence of the Herschel Sill (Fig. 1). In the period of 1952–1970, mean retreat of -0.9 ± 0.4 m \cdot a $^{-1}$ was followed by -0.8 ± 0.5 m \cdot a $^{-1}$ (1970–2000), accelerating to -1.0 ± 0.5 m \cdot a $^{-1}$ in 2000–2011. The greatest shoreline retreat occurred in the eastern portion of CR2, gradually decreasing to the west (Fig. 6). The westernmost part of CR2 is marked by deeply incised gullies. In addition, a large

Table 3 Summary of shoreline change in terms of end point rates (EPR) and area. The linear regression rate (LRR) of shoreline change (m \cdot a $^{-1}$) for different time periods and coastal reaches. Long-term shoreline movement is given as a linear regression rate (LRR) that includes all time steps

CR	1952–1970			1970–2000			2000–2011			1952–2011		
	EPR mean (m \cdot a $^{-1}$)	EPR range (m \cdot a $^{-1}$)	area (ha)	EPR mean (m \cdot a $^{-1}$)	EPR range (m \cdot a $^{-1}$)	area (ha)	EPR mean (m \cdot a $^{-1}$)	EPR range (m \cdot a $^{-1}$)	area (ha)	LRR mean (m \cdot a $^{-1}$)	LRR range (m \cdot a $^{-1}$)	area (ha)
1	-2.1 ± 0.4	-3.4 to -1.3	-7.34	-1.2 ± 0.5	-2.5 to -0.2	-2.01	-1.8 ± 0.6	-3.4 to -0.2	-3.58	-1.5 ± 0.4	-2.2 to -0.8	-17.60
2	-0.9 ± 0.4	-2.1 to -0.4	-1.33	-0.8 ± 0.5	-2.0 to -0.1	-3.07	-1.0 ± 0.5	-3.5 to -0.3	-1.41	-0.8 ± 0.5	-1.9 to -0.2	-5.76
3	-1.4 ± 0.6	-2.1 to -0.4	-1.49	-1.7 ± 0.7	-2.5 to -0.1	-3.65	-4.0 ± 1.1	-5.5 to -1.0	-2.85	-1.8 ± 0.7	-2.5 to -0.4	-7.99
4	0.2 ± 1.2	-2.3 to 1.7	-1.16	0.9 ± 0.8	0.1 to 2.7	1.84	-1.7 ± 1.7	-3.9 to 1.3	1.28	0.4 ± 0.5	-0.4 to 1.1	0.83
5	-0.1 ± 0.7	-0.7 to 1.6	-0.03	-0.3 ± 0.1	-0.5 to 0.2	-0.23	-0.1 ± 0.5	-0.7 to 0.7	-0.03	-0.2 ± 0.2	-0.4 to 0.5	-0.29
6	-0.5 ± 0.1	-0.6 to -0.4	-0.20	-0.3 ± 0.2	-0.7 to -0.1	0.02	-0.3 ± 0.1	-0.5 to 0.3	-0.12	-0.1 ± 0.2	-0.5 to 0.1	-0.37
7	0.6 ± 0.2	0.4 to 1.2	0.38	-0.1 ± 0.2	-0.3 to 0.3	0.03	-0.3 ± 0.1	-0.6 to 0.3	-0.17	0 ± 0.1	-0.1 to 0.1	0.11
All	-0.6 ± 0.5	-3.4 to 1.7	-11.16	-0.5 ± 0.4	-2.5 to 2.7	-7.06	-1.3 ± 0.7	-5.5 to 1.3	-6.88	-0.6 ± 0.3	-2.5 to 1.1	-31.07

Extremes are in bold type

Fig. 6 **a** Spatial distribution of EPRs shown as transects used in the analysis clipped to the extent of shoreline change and classified according to the rate of change. **b** Boxplots showing shoreline retreat within coastal reaches for different time periods. The end point rates (EPR) indicate rates between two time periods, while the linear regression rate (LRR) includes all time periods in the study



thermokarst feature, as well as a number of smaller ones, was active in the 1970 imagery. These features were eroded or enlarged in the 2000 and 2011 imagery. CR2 underwent ubiquitous retreat over the period of the study, with an area loss of 5.8 ha. The only excursions of the shoreline were caused by mud lobes deposited by gully streams at the base of the cliffs or by block failure of the cliffs.

CR3 encompasses the alluvial fan shoreline. This section of coast underwent the most extensive erosion over the period of the study. Overall, the shoreline retreated up to 152.7 or 108.7 ± 26.1 m on average over the study period, culminating in a net area change of almost -8 ha. Erosion rates consistently increased from -1.4 ± 0.6 to -1.7 ± 0.7 to -4.0 ± 1.1 m a⁻¹, for periods 1952–1970, 1970–2000, and 2000–2011, respectively. The highest mean retreat of this study occurred in CR4 in the period of 2000–2011, retreat rates reaching -5.5 m a⁻¹. Spatially, the greatest retreat occurred in the western portion in 1952–1970, at the transition of cliff and alluvial fan, and decreased to the west and east (Fig. 6a). The erosional hotspot migrated west in the following periods. In 1970–2000, the area loss was spread over a wider area, with the greatest retreat in the central portion. In 2000–2011, erosion was highest in the central and eastern portions of CR3, decreasing to the east, and less to the west, as CR4 experienced drastic shoreline advance.

CRs 4–5 represent the exposed and protected shorelines of Simpson Point. These coastal sections underwent the most complex changes. The western spit terminus advanced 62.7 m from 1952 to 1970 (3.5 m a⁻¹), another 130.6 m (4.3 m a⁻¹) from 1970 to 2000 (Fig. 5b). The spit morphology in 2000 suggests recent breaching of the spit and its highly dynamic non-linear nature. In the period of 2000–2011, the spit retreated 54.7 m (-5.0 m a⁻¹). These changes profoundly

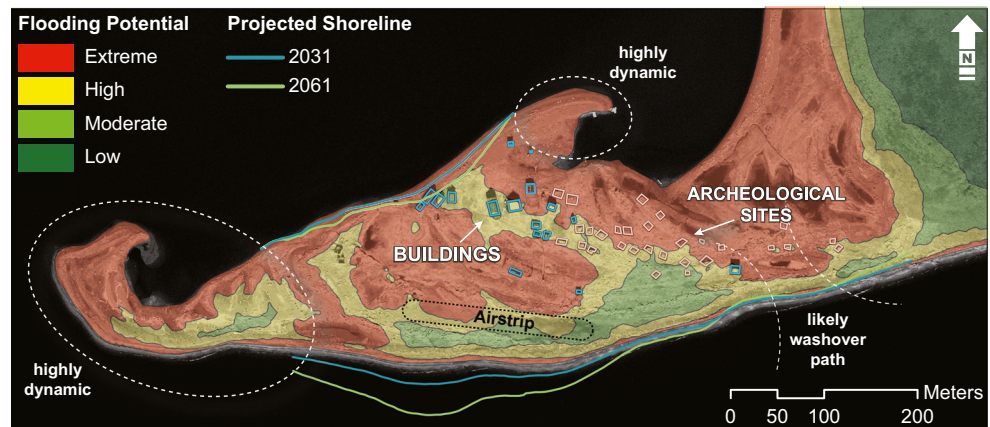
affected shoreline dynamics in CRs 4 and 5. The shoreline in CR4 rapidly prograded in the periods of 1952–1970 and 1970–2000 with mean EPRs of 0.2 ± 1.2 and 0.9 ± 0.8 m a⁻¹, respectively. However, both advance and retreat occurred in these time periods, although advance dominated in 1970–2000 and 2000–2011, expressed in net area gains of 1.84 and 1.28 ha, respectively. The eastern portion of CR4 experienced some of the most rapid retreat recorded in this study (< -3.9 m a⁻¹) in 2000–2011 that offset modest accretion in the western portion resulting in a mean shoreline change of -1.7 ± 1.7 m a⁻¹. The spit shoreline advances west of an inflection point located approximately at the center of CR4, while erosion prevails to the east.

In CR5, two inflection points delimit regions of accretion, with erosion occurring in between. The erosional hotspot followed the extension of the spit to the west. CR5 is characterized by modest retreat in all time periods of the study ranging from -0.3 to -0.1 m a⁻¹ (Table 3, Fig. 6b), also reflected in net area loss across all time periods; however, western and eastern portions of CR5 have advanced moderately over the period of the study. The storehouses located approximately in the middle of CR5 are located in the part of CR5 with the most rapid retreat.

Mapping the shoreline on the beach corresponding to CR6 was challenging. Image contrast, typically clear water and a gentle rise of the foreshore, complicated the identification of the wet-dry line. The results indicate CR6 is largely retreating, with rates ranging from -0.5 to -0.3 m a⁻¹.

The shoreline position in CR7 underwent little change over the time period. Mass movements and gully deposition at the base of the coastal bluffs mask coastal retreat. This draws attention to a potentially unique aspect of permafrost coasts linked to backshore and onshore changes in permafrost

Fig. 7 Coastal geohazard map indicating flooding potential, historic, and projected shorelines and dynamic areas with high hazard potential. These semi-transparent layers are superimposed on the 2011 image. Locations of buildings and archeological sites are highlighted as blue and peach rectangles



conditions triggered by coastal retreat. Since the period of 1950–1970, CR7 has been undergoing accelerating retreat, with rates approximately $-0.3 \text{ m}\cdot\text{a}^{-1}$.

Retreat rates calculated using the linear regression method incorporating shoreline positions from all time periods of the study are typically more conservative than EPRs from 1970 to 2000 and 2000–2011.

Hazard Assessment

The cost distance analysis produced a map which indicates that the most of the spit area has an extremely high flooding potential, with a significantly lower portion of the area classified with high and moderate potentials (Fig. 7). There are no areas located on the spit where the flooding potential was ranked as low. The classes were defined based on IPCC projections of sea level rise for years 2031 and 2061, while elevations from 0 to 0.36 m, classified as having extreme flooding hazard potential, incorporated elevations below the IPCC estimates to the target dates. The map is annotated to indicate highly dynamic areas and the location of a likely washover path. These areas should be considered highly hazardous by default. Using the LRR in CR4 and CR5, shoreline positions were projected for years 2031 and 2061, 20 and 50 years into the future, respectively.

Discussion

Shoreline Dynamics

A comparison of mean shoreline movement within CRs across the time periods studied (Fig. 6b) reveals two main patterns: CR1, CR2, CR4, and CR6 experienced intense erosion in the 1952–1970 period, decreasing in the period of 1970–2000, to significantly increase in the period of 2000–2011. A steady and statistically significant acceleration, albeit of different magnitude, took place in CR3 and CR7. In

general, a significant acceleration of coastal retreat took place in all coastal reaches in the period 2000–2011, with the exception of CR5 (Figs. 5b and 6b). Spatial patterns are also apparent where shorelines in protected coastal sections (CRs 5–7) changed little, while the shoreline in exposed coastal reaches retreated drastically (Fig. 6a). The spit shorelines were most dynamic, especially the south-oriented shore (CR4).

Temporal trends follow the previous study by Lantuit and Pollard (2008), who found that the mean rate of coastal retreat in 1952–1970 decreased in comparison with 1970–2000. A direct comparison of current erosion rates with the aforementioned study is confounded because the respective studies have a different spatial extent and resolution. In contrast to the previous study, our study employed a 5-m transect spacing (versus 300 m), investigated a smaller area, and included the shorelines of Simpson Point and the adjacent alluvial fan (CR3). In contrast to other shoreline sections, the rate of retreat increased across all time periods for CR3. Nevertheless, retreat rates and erosional trends presented by this study are generally in agreement with similar studies from the region (Héquette and Barnes 1990; Lantuit and Pollard 2003, 2008; Solomon 2005). Clearly, the inclusion of coastline sections not addressed in the previous study presents a more detailed analysis of shoreline change on Herschel Island, echoing previous research which recognized that local conditions result in significant spatial variability present within and among different reaches (Harper 1990; Jones et al. 2009; Solomon 2005). In the present study, absolute retreat rates among reaches may vary up to factor 46 and up to factor 25 within reaches in this study. Spatially dependent morphodynamic factors, such as the degree of exposure to waves, extreme events and their return frequency, ice processes, lithology, ice content, and offshore geological features, may help explain different erosion patterns evident herein.

Héquette and Barnes (1990) attempted to explain coastal bluff retreat in the Beaufort Sea as a function of different parameters (e.g., ground ice content, wave energy, sediment texture, cliff height, shoreface gradient) and found that only

ice content and wave energy correlated weakly with coastal retreat. CR1, CR2, CR3, and CR7 constitute ice-rich portions of the shoreline in the present study. In maps of ground ice distribution on Herschel Island, Bouchard (1974) indicated that S, SSE, and SE sections are ice-rich and the NE shore as not ice-rich. In addition, Pollard (1990) reported that large tabular ice bodies characterized the SE-oriented shore, with ice contents of up to 60–70 % by volume in the upper 10–15 m, while exposures on the NE-oriented shoreline were smaller and less continuous. Far lower ice-contents are suggested by recent data (Fritz et al. 2011). Nevertheless, retrogressive thaw slumps are common on SE-oriented coastlines, features that are characteristic of ice-rich permafrost (Pollard 2005). Lantuit and Pollard (2008) found the greatest erosion rates on shorelines oriented NW, NNW, and N, as these are most exposed to storms, which originate in the northwest in the southern Canadian Beaufort Sea (Hudak and Young 2002); the retreat, however, decelerated in the period 1970–2000 for most shoreline orientations, while a slight acceleration was recorded for shorelines oriented S and SW. The influence of wave energy, and perhaps ice-content, is evident in consistently high erosion rates in CR1. This coastal section is most exposed to NW storms in the current study, and the rate of coastal retreat decreased by almost half from the 1952–1970 to the 1970–2000 periods. This trend may be explained by a decrease in storm activity in the region since 1980 (Lantuit and Pollard 2008 and references therein).

Ice processes acting on the shoreface may also amplify coastal retreat in CR1. Héquette and Barnes (1990) classify the shoreface according to geomorphic processes into four zones. The fore-shore zone at the bluff toe is dominated by thermal and wave erosion. The nearshore zone up to ~6 m depth is dominated by waves and currents. The upper shoreface from 6 to 9 m depth is characterized by accretion through ice pileup and ice push-up, while the lower shoreface is dominated by ice gouging. Ice gouging leads to erosion of the lower shoreface and forces coastal retreat as the equilibrium profile is disturbed. The highest densities of ice gouges are found seaward of the landfast ice limit, which in the Beaufort Sea approximates the 20-m isobath paralleling the NE shoreline of Herschel Island and extending along Herschel Sill (Mahoney et al. 2014; Reimnitz et al. 1978). Therefore, the presence of Herschel Sill may shield coastal reaches west of CR1 from ice gouging. The rate of retreat in CR2 is typically half the mean rate in CR1 and changed little from 1952 to 1970 to the 1970–2000 period, contradicting the previous study by Lantuit and Pollard (2008). This may be an artifact of a smaller study area in the current study. Lantuit and Pollard (2008) found accelerating erosion in S- and SW-oriented shorelines and explained it in terms of a secondary preferential direction of storms from the SE and SSE (Harper and Penland 1982) and by the concentration of massive ice along these shorelines. The number of retrogressive thaw slumps increased by 61 % from 1952 to 2000 (Lantuit and Pollard 2008). We also

observed similar landscape changes in aerial imagery used in this study, as mentioned in “[Shoreline Movement](#)” and indicated by the shoreline position in Fig. 5a. Thermoabrasion of sediments is enhanced by the presence of large quantities of massive ground ice (Kobayashi 1985; Aré 1988; Héquette and Barnes 1990). Furthermore, thaw subsidence of 20 m or more can be induced by melting of ground ice in a retrogressive slump headwall, while the overall cohesiveness of sediments is reduced and thus more easily eroded (Lantuit and Pollard 2008). High and increasing erosion in CR3 agrees with the previous study and may be explained in similar terms, taking into account the lower elevation and absence of massive ice. In CR3, the presence of standing water, along with active drainage and high ground ice contents, potentially renders this part of the coast most sensitive to erosion. Shoreline retreat rates in CR4 exhibited the highest variability (both within and among all time periods), reflecting the dynamic nature of the spit and its morphodynamic dependence on the adjacent CR3. Shoreline stability in CR7 is a function of denudational processes affecting the hinterland, with accompanying deposition on the bluff toe. A more thorough analysis of ground ice distribution, nearshore parameters, and a comprehensive analysis of storm climatology should be undertaken to explain the spatial and temporal variations more accurately.

The acceleration of shoreline change rates found in this study agrees with results by other studies in the Alaskan Beaufort Sea (e.g., Barnhart et al. 2014a; Jones et al. 2009; Mars and Houseknecht 2007). No increase in overall storm frequency, which could explain these findings, could be identified by previous studies, although there are no studies that match the time period in the current study (Hudak and Young 2002). However, storms in the Beaufort Sea are more frequent in late summer and early fall (Atkinson 2005). In addition, landfast ice breakup and ice-free conditions in the Beaufort Sea occurred 19 and 39 days earlier, respectively, in the period 2000–2007 than in 1973–1977 (Mahoney et al. 2014). Duration of wave setup and increased wave height show significant positive trends as the length of the open water season in the Beaufort Sea increased by factor 1.9 from 1979 to 2012 (Barnhart et al. 2014b). The lengthening open water season resulted in anomalously high surface water temperatures in the most of the Arctic Ocean including the Beaufort Sea (Steele et al. 2008), which is another factor that drives erosion of ice-rich permafrost coasts (Aré 1988; Barnhart et al. 2014a; Kobayashi et al. 1999; Ravens et al. 2012) and may help explain the accelerating trend observed by the current study. These changes result in increasing vulnerability of Arctic coasts to erosion (Barnhart et al. 2014b).

Coastal Evolution

Our analyses indicate erosion is widespread in the study area. It is likely that the trends in shoreline dynamics will continue in the future as well. Based on the LRR for the period 1952–

2011, we projected the shoreline 20 and 50 years into the future. The LRR is susceptible to outlier points and clustered data and was chosen because the time step between the last two data points is small; therefore, these points should have a greater influence on the LRR and better reflect recent conditions. All data points were used in statistical summaries of the LRR. (e.g., Dolan et al. 1991). It must be emphasized, however, that our analyses are based on the assumption of linearity of coastal processes, such as SLR and wave intensity. Given that we found an intensification of coastal erosion over the period of the study, the projected shorelines represent a very conservative estimate of future shoreline position, as they are consistently lower than the EPR from 2000 to 2011, at least along the shorelines of CRs 1–4. The assumption of linearity may not be appropriate given the non-linear predictions of climate change in the Arctic, including a lengthening of the open water season duration and sea ice decline, leading to a positive influence on the wave climate (Church et al. 2013; Thomson and Rogers 2014) that coincides with the period of increased storm frequency (Atkinson 2005). As an overall increase in the frequency of extreme events is expected (Lambert 2004), and long-term SLR affects the Beaufort Sea (Manson and Solomon 2007), increasing erosion of the Beaufort Sea coast is almost certain (Jones et al. 2009; Manson and Solomon 2007; Overeem et al. 2011).

These changing environmental factors will affect the evolution of Simpson Point, as well. The gravelly spit was relatively stable over the study period, with aggradation in CR4, modest erosion in CR5, and an increase in overall length. The excursion of the spit terminus in 2000 probably resulted from breaching during a storm event and subsequent adjustment. Ample sediment supply indicated by high updrift erosion rates allowed the spit to increase in width, with minor retreat of the spit terminus position in 2000. The inflection point located roughly in the middle of CR4 seems to originate from a morphodynamic feedback of spit growth, and at least to some extent, the different compositions of CR3 and CR4. As erosion continued to the east, the inflection point migrated west and will likely continue, as the shoreline adjusts to the changing coastal setting. Sediment supply does not seem to be a limiting factor for spit growth; however, changing environmental parameters may increase the frequency of coastal flooding and overwash (Manson and Solomon 2007; Walsh et al. 2010) and affect ice processes (e.g., ride-up and push-up).

Ice pileup and push-up are processes of beach nourishment in Arctic regions (Reimnitz et al. 1990) that are active on Simpson Point. Ice push-up transports sediments from the shoreface, depositing them on the beach and creating distinctive pile-up mounds, while ice ride-up refers to the landward sliding of an ice sheet across the beach. These processes are active mainly when the sea is frozen or transitions to frozen. Poorly sorted, semi-linear hummocky melt-lag deposits found

on the spit testify to the effects of these processes. Although they are commonly reworked by waves, these deposits provide at least some protection from wave attack and storm surge. Reimnitz et al. (1990) report that pileups were more frequent earlier in the century when fetch was shorter, yet it is unclear how these ice processes will be affected as environmental changes proceed.

Another caveat in the evolution of Simpson Point in light of ongoing transgressive forcing is the effect of increased coastal flooding and overwash frequency. Sallenger Asbury (2000) described four regimes of storm impact on sandy barrier islands whereby run-up and foredune or berm crest elevation are the main components. Orford (2011) proposed a similar impact scale recognizing the distinct morphodynamic characteristics of gravelly barriers. Apart from total barrier inundation and removal, the morphodynamic process-response is still not well understood. In a rare example of gravelly beach dynamics in the Arctic, beaches in the resolute area have shown some resilience to moderate storms (St-Hilaire-Gravel et al. 2012). Critical to the morphodynamic response is the return period of extreme water elevations (Forbes et al. 1995; Matias et al. 2012; Orford and Anthony 2011), which has been demonstrated on sandy barriers (e.g., Claudino-Sales et al. 2008; Morton et al. 1994). Substantial reworking of sediments is possible when critical stability thresholds are exceeded, or sediment supply is interrupted (Matias et al. 2012). However, if the sediment supply for Simpson Point is not interrupted, moderate storms overtopping the barrier crest may increase the resilience of the barrier as the wave run-up will act to build up the barrier crest (Matias et al. 2012; Orford et al. 1991; Orford and Anthony 2011). The low elevations of Simpson Point, and observed washover deposits, point to the high potential of overtopping and washover. The eastern portion of CR4, especially, is being eroded quickly toward the low-lying wetland backbarrier. This area should be considered as having a high hazard potential of breaching and washover. However, in the absence of tide data at Simpson Point and run-up and swash models for the site and the dearth of comparative studies in the Arctic, stability thresholds remain a question for further studies. Ice and overwash processes may adversely affect the infrastructure on the spit. However, they are part of the life cycle of an Arctic barrier, allowing for lateral and vertical accretion as sediments are delivered to the backshore and the barrier platform.

Geohazard Mapping

In “[Hazard Assessment](#),” we presented a map indicating future shoreline positions and flooding hazard created in the course of the study. This map identifies infrastructure or archeological sites likely vulnerable to these hazards (Fig. 7). However, these analyses require a number of considerations.

Shoreline projections do not take into account morphological changes caused by future storm events that may punctuate the evolution of the spit. The flooding hazard assessment also does not consider event-related factors such as wave run-up levels or storm surge nor does it consider factors that may impede the propagation of a flood (i.e. surface roughness, permeability, etc.). Likewise, morphological changes to the beachface and berm during an event are not considered. Furthermore, fundamental data, such as surge return period, the potential for barrier washover, or even the elevation of mean sea level, are not established at the study site and complicate validation of the presented model. Even though there are considerable differences in methodology and data quality with the current study, a recent study employed a similar flood mapping approach to qualitatively validate a storm impact in their study area and found good agreement between observed and predicted impacts (Perini et al. 2015).

The cost distance analysis honors cell connectivity (lateral and diagonal) (Adriaensen et al. 2003) so that the model is superior to the “bathtub” models of inundation, in which contours below a projected sea level were flooded regardless of connectivity (e.g., Moorhead and Brinson 1995; Titus and Richman 2001). However, connectivity in our analysis may overestimate flooding (Poulter and Halpin 2008). Therefore, our type of geohazard analysis necessitates further improvement in comparison to other coastal geohazard maps (e.g., Perini et al. 2015; TAMUCC-HRI 2014). Rather than predicting impacts of flood events, the map illustrates areas that could be affected by flood levels matched to current IPCC estimates of sea level rise. This analysis does provide insight into the existing hazard potential and can be of use to stakeholders, archeologists, and park management. The historical buildings close to the shore on the north side of Simpson Point are at risk of being undermined by coastal erosion. It is clear, however, that due to the low elevation, coastal flooding threatens most of the spit. The areas mapped as having an extreme flood potential fall below even the 20- and 50-year estimates of sea level in IPCC RCPs (>0.36 m). SLR and more frequent extreme events will increase the frequency of flooding of the spit even further.

Conclusions

The present study investigated shoreline dynamics of the eastern tip of Herschel Island, with a focus on a gravelly spit, Simpson Point, where we assessed coastal hazards stemming from shoreline retreat and coastal flooding. Herschel Island is a candidate for a UNESCO world heritage site. Our analyses demonstrate Simpson Point is vulnerable to sea level rise, like many world heritage sites around the world (Marzeion and Levermann 2014), although this has previously not been documented in the Arctic.

Shoreline retreat was assessed based on aerial photographs for the periods 1952–1970, 1970–2000, and 2000–2011. Our analyses reveal that the study area is undergoing widespread shoreline retreat. The mean rate of shoreline movement decreased from -0.6 ± 0.5 to -0.5 ± 0.4 $\text{m}\cdot\text{a}^{-1}$ in the periods of 1952–1970 and 1970–2000, respectively, increasing to -1.3 ± 0.7 $\text{m}\cdot\text{a}^{-1}$ in the period 2000–2011. Coastal sections with the highest wave exposure and ice content had the highest rates of erosion. Very high retreat rates (up to -4.0 $\text{m}\cdot\text{a}^{-1}$) affected CR3, an alluvial fan with active drainage and waterlogged soils. Shoreline movement on coastal sections located on the coarse clastic spit showed the highest variability.

We present a map featuring future shoreline positions 20 and 50 years in the future and classified flood hazard potential on a cost distance surface according to IPCC projections of sea level rise for the same time periods. The resulting coastal geohazard indicates that coastal hazards on Simpson Point are less related to coastal retreat, but flooding, combined with transgressive forcing and climate change (e.g., increased occurrence of extreme events), poses serious threats to this site. The findings of this study may be applicable to similar sites in the Arctic (e.g., Shingle Point). The conditions described by our analyses raise questions regarding risk mitigation. The first step in risk mitigation is achieved by defining vulnerable areas and appropriately managing these areas. Hazard reduction measures fall into two main categories: non-structural and structural measures (Danard et al. 2003). Non-structural measures include not only relocation and land use regulation but also soft-armoring approaches such as beach nourishment. Structural measures include the use of sea walls, dikes, groins, flood-proofing, and storm surge-resistant construction. Given the remoteness and associated construction costs in the study area, many of these options are not viable. A mitigation strategy, therefore, should include a combination of these approaches; however, it must be in close consultation with the Inuvialuit for whom Herschel Island is an important cultural and historic site. A mitigation strategy should reflect Inuvialuit attitudes toward land use, burial and spiritual sites, and historical and cultural sites. For example, grave sites are not to be disturbed, and nature should be allowed to take its course (Inuvik Community Corporation, Tuktuuyaqtuq Community Corporation, and Aklavik Community Corporation 2006, pp. 8–1). Therefore, our recommendation is to relocate and elevate those historic buildings acutely at risk. Part of the strategy should include the prioritization of archeological investigations. These efforts would ensure that the historical and cultural heritage of Simpson Point is protected and preserved for future generations compatible with traditional values, even though the spit will experience increased flooding recurrence.

Acknowledgments We are grateful to the Yukon Territorial Government, Yukon Parks (Herschel Island Quiqiktaruk Territorial Park), and the Aurora Research Institute for their support during this project. This work was funded

by the Helmholtz Association (grant no. VH-NG-801 to Hugues Lantuit). We would like to thank Michael Krautblatter, George Tanski, Frank Günther, Samuel Stettner, Stefanie Weege, and Juliane Wolter for their help in the field and in the lab; Clara Amaroli, Lee John Meyook, Edward McLeod, and Richard Gordon for their feedback on the flooding potential map; Laura Elena Kelvin and Max Friesen for their clarification of Inuvialuit interests; and many more who made this project possible.

Open Access This article is distributed under the terms of the Creative Commons Attribution 4.0 International License (<http://creativecommons.org/licenses/by/4.0/>), which permits unrestricted use, distribution, and reproduction in any medium, provided you give appropriate credit to the original author(s) and the source, provide a link to the Creative Commons license, and indicate if changes were made.

References

- Adriaensens F., J.P. Chardon, G. De Blust, E. Swinnen, S. Villalba, H. Gulinck, and E. Matthysen. 2003. The application of “least-cost” modelling as a functional landscape model. *Landscape and Urban Planning* 64: 233–247. doi:10.1016/s0169-2046(02)00242-6.
- Aré F.E. 1988. Thermal abrasion of sea coasts (part I). *Polar Geography and Geology* 12: 1–1. doi:10.1080/10889378809377343.
- Atkinson David E. 2005. Observed storminess patterns and trends in the circum-Arctic coastal regime. *Geo-Marine Letters* 25: 98–109. doi:10.1007/s00367-004-0191-0.
- Barnhart Katherine R., Robert S. Anderson, Irina Overeem, Cameron Wobus, Gary D. Clow, and Frank E. Urban. 2014a. Modeling erosion of ice-rich permafrost bluffs along the Alaskan Beaufort sea coast. *Journal of Geophysical Research: Earth Surface* 119: 1155–1179. doi:10.1002/2013jg002845.
- Barnhart K.R., I. Overeem, and R.S. Anderson. 2014b. The effect of changing sea ice on the vulnerability of Arctic coasts. *The Cryosphere Discussions* 8: 2277–2329. doi:10.5194/tcd-8-2277-2014.
- Bouchard Michel. 1974. *Surficial geology of Herschel Island, Yukon Territory*. M.S. Thesis, Montréal, Québec: Université de Montréal.
- Burn C.R., and Y. Zhang. 2009. Permafrost and climate change at Herschel Island (Qikiqtaruq), Yukon Territory, Canada. *Journal of Geophysical Research* 114. doi:10.1029/2008JF001087.
- Carter R.W.G., and J.D. Orford. 1993. The morphodynamics of coarse clastic beaches and barriers: a short-and long-term perspective. *Journal of Coastal Research*: 158–179.
- Church, J.A., P.U. Clark, A. Cazenave, J.M. Gregory, S. Jevrejeva, A. Levermann, M.A. Merrifield, et al. 2013. *Sea level change*. Climate change 2013: The physical science basis. Working group I contribution to the fifth assessment report of the Intergovernmental Panel on Climate Change. Cambridge, United Kingdom: Intergovernmental Panel on Climate Change-IPCC, C/O World Meteorological Organization, 7bis Avenue de la Paix, CP 2300 CH-1211 Geneva 2 (Switzerland).
- Claudino-Sales Vanda, Ping Wang, and Mark H. Horwitz. 2008. Factors controlling the survival of coastal dunes during multiple hurricane impacts in 2004 and 2005: Santa Rosa barrier island, Florida. *Geomorphology* 95: 295–315. doi:10.1016/j.geomorph.2007.06.004.
- Couture N.J., M.R. Craymer, D.L. Forbes, P.R. Fraser, J.A. Henton, T.S. James, K.A. Jenner, et al. 2013. Coastal geoscience for sustainable development in Nunavut: 2013 activities. *Summary of Activities*: 139–148.
- Danard Maurice, Adam Munro, and Tad Murty. 2003. Storm surge hazard in Canada. *Natural Hazards* 28: 407–434. doi:10.1023/A:1022990310410.
- Dolan Robert, Michael S. Fenster, and Stuart J. Holme. 1991. Temporal analysis of shoreline recession and accretion. *Journal of Coastal Research* 7: 723–744.
- Dumas Jacqueline, Eddy Carmack, and Humfrey Melling. 2005. Climate change impacts on the Beaufort shelf landfast ice. *Cold Regions Science and Technology* 42: 41–51. doi:10.1016/j.coldregions.2004.12.001.
- Forbes, D. L., J. D. Orford, R. W. G. Carter, J. Shaw, and S. C. Jennings. 1995. Morphodynamic evolution, self-organisation, and instability of coarse-clastic barriers on paraglacial coasts. *Marine Geology* 126. Large-scale coastal behavior: 63–85. doi: 10.1016/0025-3227(95)00066-8.
- Forbes D.L. 2011. *State of the Arctic coast 2010: scientific review and outlook*. Geesthacht: International Arctic Science Committee, Land-Ocean Interactions in the Coastal Zone, Arctic Monitoring and Assessment Programme, International Permafrost Association. Helmholtz-Zentrum.
- Foster, Emmett R., and Rebecca J. Savage. 1989. Methods of historical shoreline analysis. In *Coastal Zone '89*, 4434–4448. ASCE.
- Friesen T. Max, and Charles D. Arnold. 2008. The timing of the Thule migration: new dates from the western Canadian Arctic. *American Antiquity* 73: 527–538.
- Fritz Michael, Sebastian Wetterich, Hanno Meyer, Lutz Schirmeister, Hugues Lantuit, and Wayne H. Pollard. 2011. Origin and characteristics of massive ground ice on Herschel Island (western Canadian Arctic) as revealed by stable water isotope and hydrochemical signatures. *Permafrost and Periglacial Processes* 22: 26–38. doi:10.1002/ppp.714.
- Fritz Michael, Sebastian Wetterich, Lutz Schirmeister, Hanno Meyer, Hugues Lantuit, Frank Preusser, and Wayne H. Pollard. 2012. Eastern Beringia and beyond: Late Wisconsinan and Holocene landscape dynamics along the Yukon Coastal Plain, Canada. *Palaeogeography, Palaeoclimatology, Palaeoecology* 319-320: 28–45. doi:10.1016/j.palaeo.2011.12.015.
- Füssel Hans-Martin. 2007. Vulnerability: A generally applicable conceptual framework for climate change research. *Global Environmental Change* 17: 155–167. doi:10.1016/j.gloenvcha.2006.05.002.
- Genz Ayesha S., Charles H. Fletcher, Robert A. Dunn, L. Neil Frazer, and John J. Rooney. 2007. The predictive accuracy of shoreline change rate methods and alongshore beach variation on Maui, Hawaii. *Journal of Coastal Research* 23: 87–105. doi:10.2112/05-0521.1.
- Günther F., P.P. Overduin, A. Baranskaya, T. Opel, and M.N. Grigoriev. 2013. Observing Muostakh Island disappear: erosion of a ground-ice-rich coast in response to summer warming and sea ice reduction on the East Siberian shelf. *The Cryosphere Discussions* 7: 4101–4176. doi:10.5194/tcd-7-4101-2013.
- Harper John Reed, and Shea Penland. 1982. *Beaufort Sea sediment dynamics*. Woodward-Clyde Consultants.
- Harper John R., R. Falconer Henry, and Gordon G. Stewart. 1988. Maximum storm surge elevations in the Tuktoyaktuk region of the Canadian Beaufort sea. *Arctic* 41: 48–52.
- Harper J.R. 1990. Morphology of the Canadian Beaufort Sea coast. *Marine Geology* 91: 75–91. doi:10.1016/0025-3227(90)90134-6.
- Hartmann D.L., A.M.G. Klein Tank, M. Ruscicucci, L.V. Alexander, B. Broenniman, Y. Charabi, F.J. Dentener, E.J. Dlugokencky, D.R. Easterling, and A. Kaplan. 2013. Observations: atmosphere and surface. In *Climate change 2013: The physical science basis. Contribution of working group I to the fifth assessment report of the intergovernmental panel on climate change*, eds. T.F. Stocker, D. Qin, G. Plattner, M. Tignor, S.K. Allen, J. Boschung, A. Nauels, Y. Xia, V. Bex, and P.M. Midgley, 159–254. Cambridge and New York: Cambridge University Press.
- Henry, R. F. 1975. *Storm surges*. Technical Report 19. Beaufort Sea Project. Victoria, B.C., Canada: Beaufort Sea Project, Department of the Environment.

- Héquette A., and P.W. Barnes. 1990. Coastal retreat and shoreface profile variations in the Canadian Beaufort Sea. *Marine Geology* 91: 113–132. doi:10.1016/0025-3227(90)90136-8.
- Héquette Arnaud, Marc Desrosiers, and Peter W. Barnes. 1995. Sea ice scouring on the inner shelf of the southeastern Canadian Beaufort Sea. *Marine Geology* 128: 201–219. doi:10.1016/0025-3227(95)00095-G.
- Hill P.R., P.J. Mudie, K. Moran, and S.M. Blasco. 1985. A sea-level curve for the Canadian Beaufort shelf. *Canadian Journal of Earth Sciences* 22: 1383–1393. doi:10.1139/e85-146.
- Hudak D.R., and J.M.C. Young. 2002. Storm climatology of the southern Beaufort Sea. *Atmosphere-Ocean* 40: 145–158. doi:10.3137/ao.400205.
- Huder Roger C. 2012. FEMA glossary. In *Disaster operations and decision making*, 341–361. Hoboken: Wiley.
- Inuvik Community Corporation, Tuktuuyaqtuq Community Corporation, and Aklarvik Community Corporation. 2006. *Inuvialuit settlement region—traditional knowledge report*. Calgary, Alberta: Mackenzie Project Environmental Group.
- James T.S., J.A. Henton, L.J. Leonard, A. Darlington, D.L. Forbes, and M. Craymer. 2014. *Relative sea-level projections in Canada and the adjacent mainland United States*. Natural Resources Canada/ESS/Scientific and Technical Publishing Services.
- Jones B.M., C.D. Arp, M.T. Jorgenson, K.M. Hinkel, J.A. Schmutz, and P.L. Flint. 2009. Increase in the rate and uniformity of coastline erosion in Arctic Alaska. *Geophysical Research Letters* 36. doi:10.1029/2008GL036205.
- Kobayashi, Nobuhisa. 1985. Formation of thermoerosional niches into frozen bluffs due to storm surges on the Beaufort Sea coast. *Journal of Geophysical Research: Oceans (1978–2012)* 90: 11983. doi:10.1029/jc090ic06p11983.
- Kobayashi N., J.C. Vidrine, R.B. Nairn, and S.M. Solomon. 1999. Erosion of frozen cliffs due to storm surge on Beaufort Sea coast. *Journal of Coastal Research* 15: 332–344.
- Kwok R., and D.A. Rothrock. 2009. Decline in Arctic sea ice thickness from submarine and ICESat records: 1958–2008. *Geophysical Research Letters* 36. doi:10.1029/2009GL039035.
- Lambert Steven J. 2004. Changes in winter cyclone frequencies and strengths in transient enhanced greenhouse warming simulations using two coupled climate models. *Atmosphere-Ocean* 42: 173–181. doi:10.3137/ao.420302.
- Lantuit H., P.P. Overduin, N. Couture, S. Wetterich, F. Aré, D. Atkinson, J. Brown, G. Cherkashov, D. Drozdov, and D.L. Forbes. 2012. The Arctic coastal dynamics database: A new classification scheme and statistics on Arctic permafrost coastlines. *Estuaries and Coasts* 35: 383–400. doi:10.1007/s12237-010-9362-6.
- Lantuit H., and W. Pollard. 2003. Remotely sensed evidence of enhanced erosion during the twentieth century on Herschel Island, Yukon Territory. *Berichte zur Polar- und Meeresforschung* 443: 54–59.
- Lantuit H., and W.H. Pollard. 2008. Fifty years of coastal erosion and retrogressive thaw slump activity on Herschel Island, southern Beaufort Sea, Yukon Territory, Canada. *Geomorphology* 95: 84–102. doi:10.1016/j.geomorph.2006.07.040.
- Lo C.P., K. Albert, and W. Yeung. 2007. *Concepts and techniques of geographic information systems*. Upper Saddle River, NJ: Pearson Prentice Hall.
- Mackay, J. R. 1986. Fifty years (1935 to 1985) of coastal retreat west of Tuktoyaktuk, District of Mackenzie. *Current Research, Part A, Geological Survey of Canada, Paper* 86: 1.
- Mackay J. Ross. 1959. Glacier ice-thrust features of the Yukon coast. *Geographical Bulletin* 13: 5–21.
- Mahoney Andrew R., Hajo Eicken, Allison G. Gaylord, and Rudiger Gens. 2014. Landfast sea ice extent in the Chukchi and Beaufort Seas: The annual cycle and decadal variability. *Cold Regions Science and Technology* 103: 41–56. doi:10.1016/j.coldregions.2014.03.003.
- Manson Gavin K., and Steven M. Solomon. 2007. Past and future forcing of Beaufort Sea coastal change. *Atmosphere-Ocean* 45: 107–122. doi:10.3137/ao.450204.
- Mars J.C., and D.W. Houseknecht. 2007. Quantitative remote sensing study indicates doubling of coastal erosion rate in past 50 yr along a segment of the Arctic coast of Alaska. *Geology* 35: 583–586. doi:10.1130/G23672A.1.
- Marzeion Ben, and Anders Levermann. 2014. Loss of cultural world heritage and currently inhabited places to sea-level rise. *Environmental Research Letters* 9: 034001. doi:10.1088/1748-9326/9/3/034001.
- Maslakov Alexey, and Gleb Kraev. 2014. Coastal hazards within indigenous settlements of Chukchi peninsula. In *Engineering geology for society and territory—volume 4*, eds. Giorgio Lollino, Andrea Manconi, Jacques Locat, Huang Yu, and Miquel Canals Artigas, 33–36. Cham: Springer International Publishing.
- Mason Owen K., James W. Jordan, Leanne Lestak, and William F. Manley. 2012. Narratives of shoreline erosion and protection at Shishmaref, Alaska: The anecdotal and the analytical. *Pitfalls of Shoreline Stabilization* 3: 73–92. doi:10.1007/978-94-007-4123-2_5.
- Matias Ana, Jon J. Williams, Gerhard Masselink, and Óscar Ferreira. 2012. Overwash threshold for gravel barriers. *Coastal Engineering* 63: 48–61. doi:10.1016/j.coastaleng.2011.12.006.
- Meyssignac Benoit, and Anny Cazenave. 2012. Sea level: A review of present-day and recent-past changes and variability. *Journal of Geodynamics* 58: 96–109. doi:10.1016/j.jog.2012.03.005.
- Moorhead Kevin K., and Mark M. Brinson. 1995. Response of wetlands to rising sea level in the lower coastal plain of North Carolina. *Ecological Applications* 5: 261–271. doi:10.2307/1942068.
- Morgan, E. D., L. Titus, R. J. Small, and Corony Edwards. 1983. The composition of fatty materials from a Thule Eskimo site on Herschel Island Arctic 36: 356–360. doi:10.14430/arctic2290.
- Morton R.A., J.G. Paine, and J.C. Gibeaut. 1994. Stages and durations of post-storm beach recovery, southeastern Texas coast, U.S.A. *Journal of Coastal Research* 10: 884–908.
- Nagy Murielle. 2012. Inuvialuit ancestors. In *In Herschel Island: a natural and cultural history of Yukon's Arctic island = Qikiqtaryuk*, ed. Christopher Robert Burn. Whitehorse: Wildlife Management Advisory Council (North Slope).
- Obu, Jaroslav, Hugues Lantuit, Isla Myers-Smith, Birgit Heim, Juliane Wolter, and Michael Fritz. 2015accepted. Effect of terrain on soil organic carbon and total nitrogen storage on Herschel Island, western Canadian Arctic. *Permafrost and Periglacial Processes*.
- Olynyk, Douglas M. 2008. Summary of the significance of and threats to cultural resources located at the historic settlement area on Herschel Island territorial park of Yukon. In *Heritage at risk: ICOMOS world report 2006/2007 on monuments and sites in danger*, ed. Michael Petzet and John Ziesemer. International council on monuments and sites (Paris). Altenburg: E. Reinhold-Verlag.
- Orford, J. D. 2011. Gravel-dominated coastal-barrier reorganisation variability as a function of coastal susceptibility and barrier resilience. In *coastal sediments*, 11:1257–1270. World Scientific Publishing Company.
- Orford Julian D., and Edward J. Anthony. 2011. Extreme events and the morphodynamics of gravel-dominated coastal barriers: Strengthening uncertain ground. *Marine Geology* 290: 41–45. doi:10.1016/j.margeo.2011.10.005.
- Orford Julian D., Richard W.G. Carter, and Simon C. Jennings. 1991. Coarse clastic barrier environments: Evolution and implications for quaternary sea level interpretation. *Quaternary International* 9: 87–104. doi:10.1016/1040-6182(91)90068-Y.
- Overduin, Pier P, Strzelecki, Mateusz C., Grigoriev, Mikhail N., Couture, Nicole, Lantuit, Hugues, St-Hilaire-Gravel, Dominique, Günther, Frank, and Sebastian Wetterich. 2014. Coastal changes in the Arctic. In: Martini, I. P. and Wanless, H. R. ed. *Sedimentary coastal*

- zones from high to low latitudes: similarities and differences. Geological Society, London, Special Publications, 388: 102–129. doi:10.1144/SP388.13.
- Overeem Irina, Robert S. Anderson, Cameron W. Wobus, Gary D. Clow, Frank E. Urban, and Nora Matell. 2011. Sea ice loss enhances wave action at the Arctic coast. *Geophysical Research Letters* 38: L17503. doi:10.1029/2011GL048681.
- Perini Luisa, Lorenzo Calabrese, Salerno Giovanni, P. Ciavola, and C. Armaroli. 2015. Mapping of flood risk in Emilia-Romagna coastal areas. *Natural Hazards and Earth System Science Discussions* 3: 4315–4352. doi:10.5194/nhessd-3-4315-2015.
- Pinchin B.M., R.B. Naim, and K.L. Philpott. 1985. *Beaufort Sea coastal sediment study: Numerical estimation of sediment transport and nearshore profile adjustment at coastal sites in the Canadian Beaufort Sea*. Geological Survey of Canada.
- Pollard, W. H. 1990. The nature and origin of ground ice in the Herschel Island area, Yukon Territory. In *Proceedings, Fifth Canadian Permafrost Conference, Québec*, 23–30.
- Pollard, W. H. 2005. Thermokarst. Edited by M. Nutall. *Encyclopedia of the Arctic*. New York: Routledge.
- Poulter B., and P.N. Halpin. 2008. Raster modelling of coastal flooding from sea-level rise. *International Journal of Geographical Information Science* 22: 167–182. doi:10.1080/13658810701371858.
- Rampton V.N. 1982. *Quaternary geology of the Yukon coastal plain*. Ottawa: Geological Survey of Canada.
- Ravens T., B. Jones, J. Zhang, C. Arp, and J. Schmutz. 2012. Process-based coastal erosion modeling for Drew Point, North Slope, Alaska. *Journal of Waterway, Port, Coastal, and Ocean Engineering* 138: 122–130. doi:10.1061/(ASCE)WW.1943-5460.0000106.
- Reimnitz Erk, Larry Toimil, and Peter Barnes. 1978. Arctic continental shelf morphology related to sea-ice zonation, Beaufort Sea, Alaska. *Marine Geology* 28: 179–210. doi:10.1016/0025-3227(78)90018-X.
- Reimnitz Erk, P.W. Barnes, and J.R. Harper. 1990. A review of beach nourishment from ice transport of shoreface materials, Beaufort Sea, Alaska. *Journal of Coastal Research* 6: 439–469.
- Romine Bradley M., Charles H. Fletcher, L. Neil Frazer, Ayesha S. Genz, Matthew M. Barbee, and Siang-Chyn Lim. 2009. Historical shoreline change, southeast Oahu, Hawaii: Applying polynomial models to calculate shoreline change rates. *Journal of Coastal Research* 25: 1236–1253. doi:10.2112/08-1070.1.
- Sallenger Asbury H. Jr. 2000. Storm impact scale for barrier islands. *Journal of Coastal Research* 16: 890–895.
- Serreze Mark C., and Roger G. Barry. 2011. Processes and impacts of Arctic amplification: A research synthesis. *Global and Planetary Change* 77: 85–96. doi:10.1016/j.gloplacha.2011.03.004.
- Shaw J., R.B. Taylor, D.L. Forbes, S. Solomon, and M.H. Ruz. 1998. *Sensitivity of the coasts of Canada to sea-level rise*. Ottawa: Geological Survey of Canada.
- Smith, C. A. S., C. E. Kennedy, A. E. Hargrave, and K. M. McKenna. 1989. *Soil and vegetation of Herschel Island, Yukon Territory. Yukon Soil Survey Report, vol. 1. Land Resource Research Centre*. Ottawa, Canada: Research Branch, Agriculture Canada.
- Solomon Steven M. 2005. Spatial and temporal variability of shoreline change in the Beaufort-Mackenzie region, Northwest Territories, Canada. *Geo-Marine Letters* 25: 127–137. doi:10.1007/s00367-004-0194-x.
- Steele Michael, Wendy Er mold, and Jinlun Zhang. 2008. Arctic Ocean surface warming trends over the past 100 years. *Geophysical Research Letters* 35: L02614. doi:10.1029/2007GL031651.
- St-Hilaire-Gravel Dominique, Donald L. Forbes, and Trevor Bell. 2012. Multitemporal analysis of a gravel-dominated coastline in the central Canadian Arctic archipelago. *Journal of Coastal Research*: 421–441. doi:10.2112/JCOASTRES-D-11-00020.1.
- Stroeve, J. C., T. Markus, L. Boisvert, J. Miller, and A. Barrett. 2014. Changes in Arctic melt season and implications for sea ice loss. *Geophysical Research Letters* 41: 2013GL058951. doi:10.1002/2013GL058951.
- Stroeve Julienne C., Vladimir Kattsov, Andrew Barrett, Mark Serreze, Tatiana Pavlova, Marika Holland, and Walter N. Meier. 2012. Trends in Arctic sea ice extent from CMIP5, CMIP3 and observations. *Geophysical Research Letters* 39: L16502. doi:10.1029/2012GL052676.
- Stroeve Julienne, Marika M. Holland, Walt Meier, Ted Scambos, and Mark Serreze. 2007. Arctic sea ice decline: Faster than forecast. *Geophysical Research Letters* 34: L09501. doi:10.1029/2007GL029703.
- TAMUCC-HRI. 2014. Geohazards of Texas barrier islands, Texas A&M University—Corpus Christi, Coastal Marine and Geospatial Lab.
- Thieler Robert E., Emily A. Himmelstoss, Jessica L. Zichichi, and Ayhan Ergul. 2009. *The Digital Shoreline Analysis System (DSAS) version 4. In 0 - an ArcGIS extension for calculating shoreline change*. U. S.: Geological Survey.
- Thomson Jim, and Erick W. Rogers. 2014. Swell and sea in the emerging Arctic Ocean. *Geophysical Research Letters* 41: 3136–3140. doi:10.1002/2014GL059983.
- Titus James G., and Charlie Richman. 2001. Maps of lands vulnerable to sea level rise: Modeled elevations along the US Atlantic and gulf coasts. *Climate Research* 18: 205–228. doi:10.3354/cr018205.
- UNESCO. 2013. Ivvavik/Vuntut/Herschel Island (Qikiqtaruk)—UNESCO World Heritage Centre.
- Walsh, John E., Oleg Anisimov, Jon Ove M. Hagen, Thor Jakobsson, Johannes Oerlemans, Terry D. Prowse, Vladimir Romanovsky, et al. 2010. Sea-level rise and coastal stability in the Arctic. Arctic Climate Impact Assessment. International Arctic Science Committee.
- Westley Kieran, Bell Trevor, M.A.P. Renouf, and Lev Tarasov. 2011. Impact assessment of current and future sea-level change on coastal archaeological resources—illustrated examples from northern Newfoundland. *The Journal of Island and Coastal Archaeology* 6: 351–374. doi:10.1080/15564894.2010.520076.